Probing grain size effect in the superelastic Ti-20Zr-3Mo-3Sn alloy using spherical nanoindentation

Y. Zhou, A. Fillon, D. Laillé, T. Gloriant

Probing grain size effect in the superelastic Ti-20Zr-3Mo-3Sn alloy using spherical nanoindentation

Y. Zhou, A. Fillon*, D. Laillé, T. Gloriant

Univ Rennes, INSA Rennes, CNRS, ISCR-UMR 6226, F-35000, Rennes, France

* Corresponding author: Amélie Fillon

Postal address: Univ Rennes, INSA Rennes, CNRS, ISCR-UMR 6226, 20 avenue des Buttes de Coësmes, CS 70839, Rennes Cedex 7, France.

E-mail address: amelie.fillon@insa-rennes.fr (A. Fillon).

Abstract

Grain size effect on superelasticity was investigated in Ti-20Zr-3Mo-3Sn alloys for the same crystallographic texture and for a broad grain size range from 7 μm to 180 μm. The dependence of superelasticity on grain size was studied by spherical nanoindentation. Results displayed the same tendency as that observed during tensile tests. The small-sized β grains favored the martensitic transformation, and exhibited the greater superelasticity. It is confirmed that spherical nanoindentation is capable of characterizing superelasticity and is sensitive enough to probe grain size effect in superelastic alloys. It is also shown that β grain size evidently affects indentation hardness and modulus.

Keywords: Titanium alloys; Nanoindentation; Grain size; Superelasticity; Stress-induced martensitic transformation.

1. Introduction

Metastable β-Ti alloys are well-known to display superelastic behavior which arises from a reversible stress-induced martensitic (SIM) transformation between the body-centered cubic (bcc) β phase and the orthorhombic α″ phase when they are deformed cyclically upon loading and unloading within the first yielding region of their macroscopic engineering tensile stress-strain curves [1, 2].

The occurrence of SIM transformation in superelastic metastable β-Ti alloys depends on: (i) the metastability of β phase determined by the concentration of alloying elements; (ii) the difference between test temperature and martensite start (Ms) temperature which determines the required driving force for the transformation; (iii) the microstructure characteristics of β phase such as crystallographic texture and grain size. The above variables are influenced mutually and reciprocally, and can be tailored by the nature and concentration of alloying elements and by the thermo-mechanical treatment conditions. For instance, addition of alloying elements strongly affects the Ms temperature and the transformation strain which arises from the lattice distortion between the parent β phase and the stress-induced α″ phase, and subsequently affects the superelastic response. It was reported that alloying with Zr and Mo elements is effective to increase the superelastic recovery strain [3, 4]. The texture control is another efficient way to improve the superelasticity since the martensitic transformation strain is strongly anisotropic and addition of a small amount of Sn, as low as 1 to 4 at. %, in metastable β-Ti alloys is favorable for developing $\langle 110 \rangle_{\beta}$

recrystallization texture which is desirable for large transformation strain and subsequently for large superelastic recovery strain [5]. Addition of Sn is also very effective at suppressing the formation of athermal ω precipitates which adversely affect the superelasticity [6]. Ti-20Zr-3Mo-3Sn (at. %, Ti2033 for short) alloy has been proposed to show excellent superelasticity, and occurrence of the reversible SIM transformation has been evidenced in this alloy system by synchrotron X-ray diffraction [7, 8].

The superelastic performances of metastable β-Ti alloys are also largely dependent on the grain size [11-13]. In the last twenty years, research topics on grain refinement in superelastic alloys have attracted much attention since combinational properties such as good superelasticity, small hysteresis (low dissipation energy), high cyclic stability and high fatigue resistance can be expected to achieve so that new potential applications can be explored [14]. An earlier study conducted by Grosdidier et al. [15] showed that reduced grain size of the parent β phase lowers the Ms temperature, and thus increases the critical stress for triggering the SIM transformation. The free energy change during such transformation is responsible for the dependence of the triggering stress on grain size [16]. Bian et al. [17] proposed that smaller grain size causes higher grain boundary constraint which restrains the shear deformation within grain interiors, and thus enhances the plasticity resistance. It has also been reported that the reduced grain size could lower the martensitic transformation strain, change the phase transformation path and improve the mechanical properties of superelastic alloys [11, 18].

Bulk mechanical properties of materials are commonly measured under uniaxial loading conditions such as uniaxial tension or compression. Recently, nanoindentation is considered as a suitable and powerful technique for the characterization of local mechanical properties and nanoscale deformation behavior owing to its capability of sensitively probing indentation responses from small volumes of materials. By coupling with electron backscattered diffraction (EBSD) analysis, nanoindentation also can be used to evaluate the superelasticity of targeted individual grains with orientation indexed by EBSD [19]. It offers an opportunity to independently investigate the influence of grain size on the superelasticity by dissociating the texture factor.

The present study establishes a correlation concerning the capability of characterizing the superelasticity between tensile testing and nanoindentation measurement, and elucidate the influence of grain size on the superelasticity, indentation hardness and modulus at local scale in the metastable β Ti2033 alloy. It would be valuable to use the coherency of superelastic characteristics measured by macroscopic tensile testing and nanoindentation technique to facilitate the evaluation of superelasticity on small-sized materials in the

absence of the ability to perform macroscopic tensile, compression or bending tests.

2. Materials and methods

The Ti2033 alloy ingots were elaborated by cold crucible levitation melting (CCLM) technique from pure metals, homogenized at 1223 K for 20 h followed by water quenching, cold-rolled into 0.5 mm thickness sheet with a thickness reduction rate of 95%, and then machined into flat tensile specimens in dog-bone shape with 3 mm × 15 mm × 0.5 mm gauge dimensions. These specimens were recrystallized at 973 K, 1073 K and 1173 K for 0.5 h, respectively, followed by water quenching to retain the metastable β phase. The specimens were denoted as Ti2033-973K, Ti2033-1073K and Ti2033-1173K. It is worth to mention that the β transus temperature of Ti2033 alloy has been detected by resistivity measurements to be 963 K [7]. After thermal treatments, the specimens were treated in an HF/ HNO_3 solution (1/1 ratio) to remove the surface oxide layer.

Macroscale mechanical properties of Ti2033 specimens were evaluated by tensile testing on an INSTRON 3369 tensile machine in a strain control mode at a rate of 10^{-4} s^{-1}. Cyclic tensile tests were conducted at room temperature with a strain increment of 0.5% by steps until an elongation of 5.0% and each step was followed by a complete stress release. The tensile direction was chosen parallel to the cold rolling direction. The grain size and crystallographic orientations of individual grains were identified by EBSD on a scanning electron microscope (SEM, JEOL JSM 7100F) equipped with an Oxford HKL EBSD system and were analyzed by the HKL Channel 5 package. The surface of the specimens was prepared by electrochemical polishing in an electrolyte composed of perchloric acid (6 vol. %) and methanol (94 vol. %) at -15 °C and 0.2 A current for 45 s. Superelastic response of the Ti2033 alloy in all heat-treated states was investigated by nanoindentation using the instrumented NHT Anton Paar nanoindentation test system. Nanoindentation measurements were performed on selected grains along the surface normal direction at different penetration depths. Spherical indenter with nominal tip radius of 50 μm was used and calibrated on fused silica sample to take into account the real shape of the tip. Individual grains with targeted orientations were located by an optical microscope attached in the instrumented nanoindentation test system, with the aid of EBSD orientation maps.

3. Results and discussion

3.1 Grain size effect on superelasticity by tensile testing

The tensile cyclic stress-strain curves of Ti2033 specimens recrystallized at 973 K,

1073 K and 1173 K for 0.5 h, respectively, are shown in Fig. 1. The stress-strain curves exhibit deformation characteristics of the double yielding and the stress hysteresis phenomenon associated with the occurrence of reversible SIM transformation between β and α" phases [20, 21], demonstrating the superelasticity in Ti2033 alloy. The stress corresponding to the first yielding denotes the critical stress for SIM transformation, σ_{SIM}, as indicated by the arrow on the cycles highlighted in red. It is noticed that the σ_{SIM} increases with increasing heat treatment temperature. The yielding for SIM transformation becomes less distinct and the σ_{SIM} cannot be well defined for Ti2033-1173K specimen. The occurrence of SIM transformation can be understood regarding the competition among different possible accommodating deformation mechanisms in metastable β phase, such as slip, twinning and SIM transformation. Thus, SIM transformation is the earlier and dominant mechanism at lower grain sizes, and at higher grain sizes the σ_{SIM} tends towards the critical stress for dislocation slips σ_{CSS}, masking the SIM transformation altogether.

As indicated in Fig. 1d, for each individual loading-unloading cycle, the maximum applied strain ($\varepsilon_{applied}$), and other four types of strain, elastic recovery strain (ε_{el}), superelastic strain (ε_{se}), total recovery strain (ε_{rec}) which is the summation of ε_{el} and ε_{se}, and permanent residual strain (ε_p) after complete unloading were evaluated from the stress-strain curves to characterize superelastic properties [5, 9].

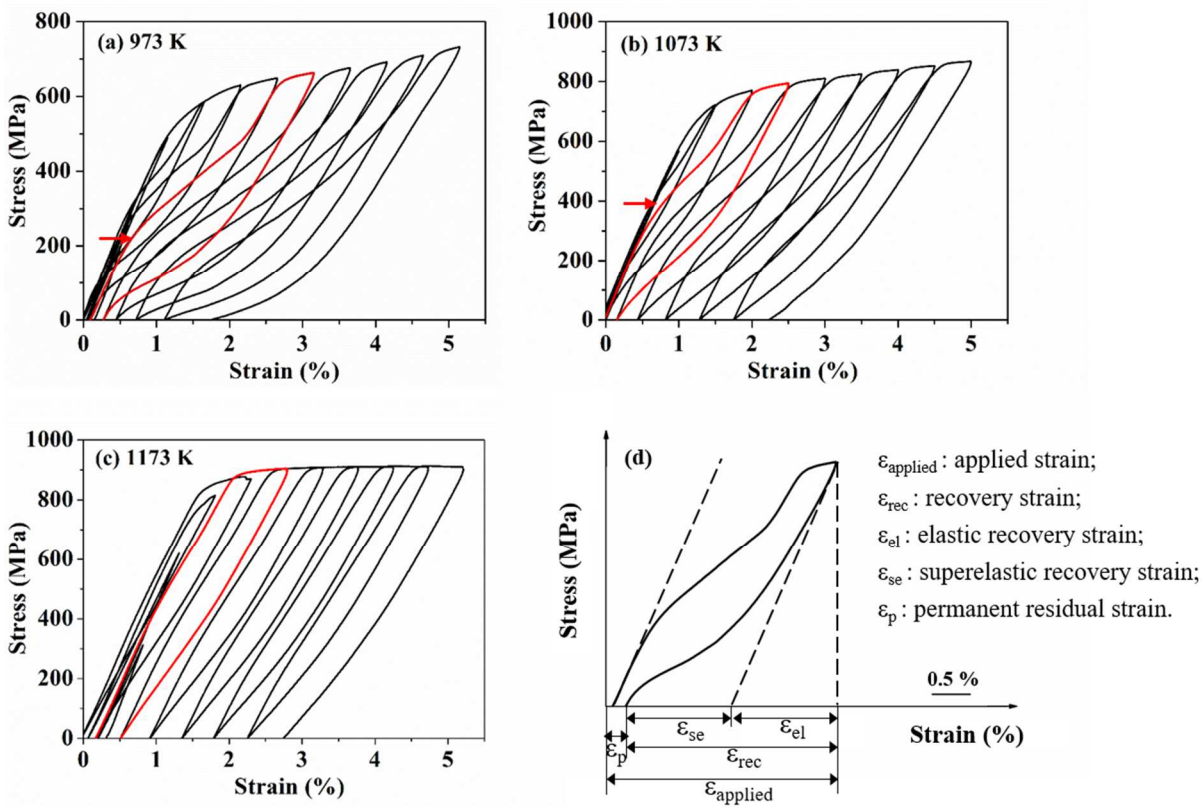

Fig. 1 Tensile cyclic stress-strain curves of Ti2033 specimens recrystallized at (a) 973 K, (b) 1073 K and (c) 1173 K for 0.5 h, respectively. The curves were reorganized from [7]. (d) measurement scheme of the

different strains from the red cycle presented in (a).

The magnitudes of total recovery strain ε_{rec} and superelastic recovery strain ε_{se} extracted from the cyclic stress-strain curves for the three specimens were plotted as a function of applied strain $\varepsilon_{applied}$ of each cycle (Fig. 2a). The diagonal line in Fig. 2a represents the 100% full recovery. Almost perfect recovery is exhibited up to 2.5% for the Ti2033-973K alloy. At high $\varepsilon_{applied}$, the deviation of ε_{rec} from the diagonal line indicates the permanently residual strain ε_p, due to the occurrence of irreversible martensitic transformation and plastic deformation. For the Ti2033-973K alloy, the total recovery strain ε_{rec} firstly increases with increasing $\varepsilon_{applied}$ until reaches the maximum ε_{rec} of 3.5% and also obtains the maximum superelastic recovery strain ε_{se} of 2.3%. ε_{rec} and ε_{se} are clearly higher than those measured for Ti2033-1073K and Ti2033-1173K alloys. The strain recovery ratios were calculated as the ratio of strain recovery to the applied strain on each cycle:

$$\eta_{\varepsilon_{rec}} = 100 * \frac{\varepsilon_{rec}}{\varepsilon_{applied}} \quad (1)$$

The variation of strain recovery ratio $\eta_{\varepsilon_{rec}}$ with respect to the applied stress $\varepsilon_{applied}$ at each cycle is presented in Fig. 2b. It shows that the three alloys follow the same tendency: the magnitudes of $\eta_{\varepsilon_{rec}}$ remain at 100% to a certain strain level and then decrease with the increasing $\varepsilon_{applied}$. It also shows that the strain recoverability is dependent on the thermal treatments. It can be concluded that by tensile testing, the recovery performances of the studied specimens behave as the following sequence: Ti2033-973K > Ti2033-1073K > Ti2033-1173K.

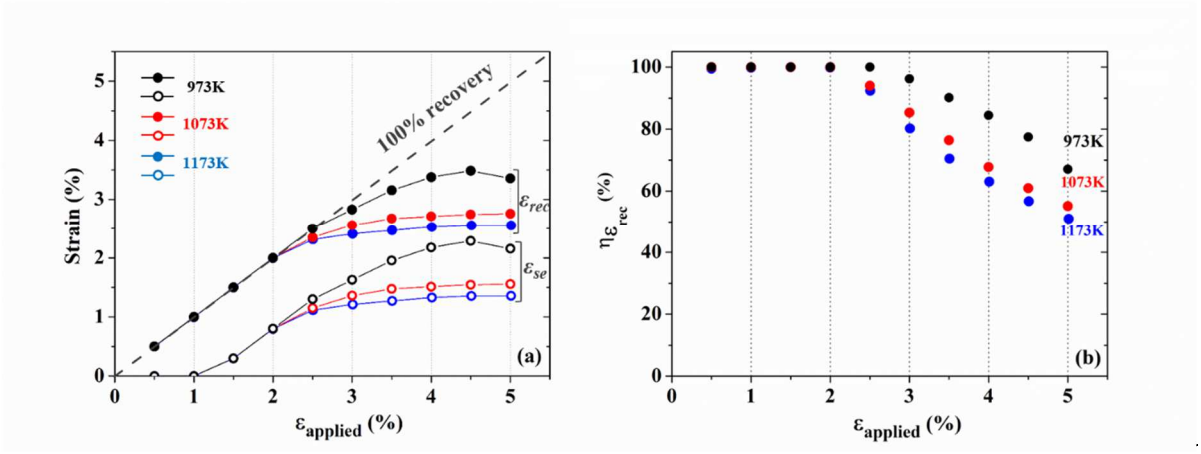

Fig. 2 (a) Total recovery strain ε_{rec}, superelastic strain ε_{se}, and (b) recovery strain ratios $\eta_{\varepsilon_{rec}}$ extracted from cyclic loading-unloading tensile curves as shown in Fig.1, and plotted as a function of the applied strain $\varepsilon_{applied}$ of each cycle.

The different levels of recoverability in superelastic alloys can be attributed as many influencing factors, such as texture [5, 7, 8, 22, 23], phase composition [5, 24],

transformation strain [23, 25], competition between the critical stresses for SIM transformation σ_{SIM} and for dislocation slip σ_{css} [13, 24, 26], and grain size [12, 13]. It is likely that the observed differences in the strain recoverability of Ti2033 alloys arise from the different heat treatments causing the difference in grain sizes. Thus, it is of great interest to elucidate the influence of heat treatment temperature on the microstructure and superelasticity of Ti2033 alloys. Fig. 3 presents the EBSD orientation maps along the normal direction (ND) for Ti2033 alloys recrystallized at 973K, 1073K, and 1173K. All specimens display typical equiaxed β-grain microstructures. The average grain size determined from the EBSD maps was calculated to be 7 μm, 70 μm and 180 μm, for the Ti2033-973K, Ti2033-1073K, and Ti2033-1173K, respectively, with standard deviation of 2 μm, 16 μm and 41 μm, respectively. That is, grain size decreases with decreasing heat treatment temperature.

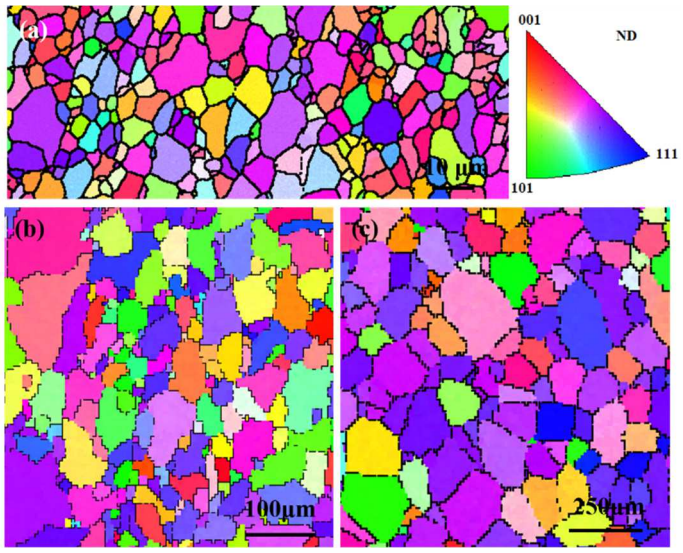

Fig. 3 EBSD orientation maps along the normal direction (ND) for recrystallized Ti2033 alloys at: (a) 973 K; (b) 1073 K; (c) 1173 K.

To furthermore compare the crystallographic orientation of the three specimens, the corresponding inverse pole figures (IPF) are shown in the rolling direction (RD) and ND for each specimen in Fig. 4. It can be seen that although the specimens were subjected to different heat treatments, all displayed the same $\{113\}_\beta$ $<110>_\beta$ strong recrystallization texture. It offers an opportunity to independently investigate the influence of grain size on the superelasticity by dissociating the texture factor. Therefore, it is reasonable to accept that during tensile test the increased superelasticity observed in the Ti2033 alloy recrystallized at lower temperature is predominantly attributed to the reduced grain size. It might be very interesting to investigate the grain size effect on superelastic behaviors of Ti2033 alloys under compression at the local scale using nanoindentation.

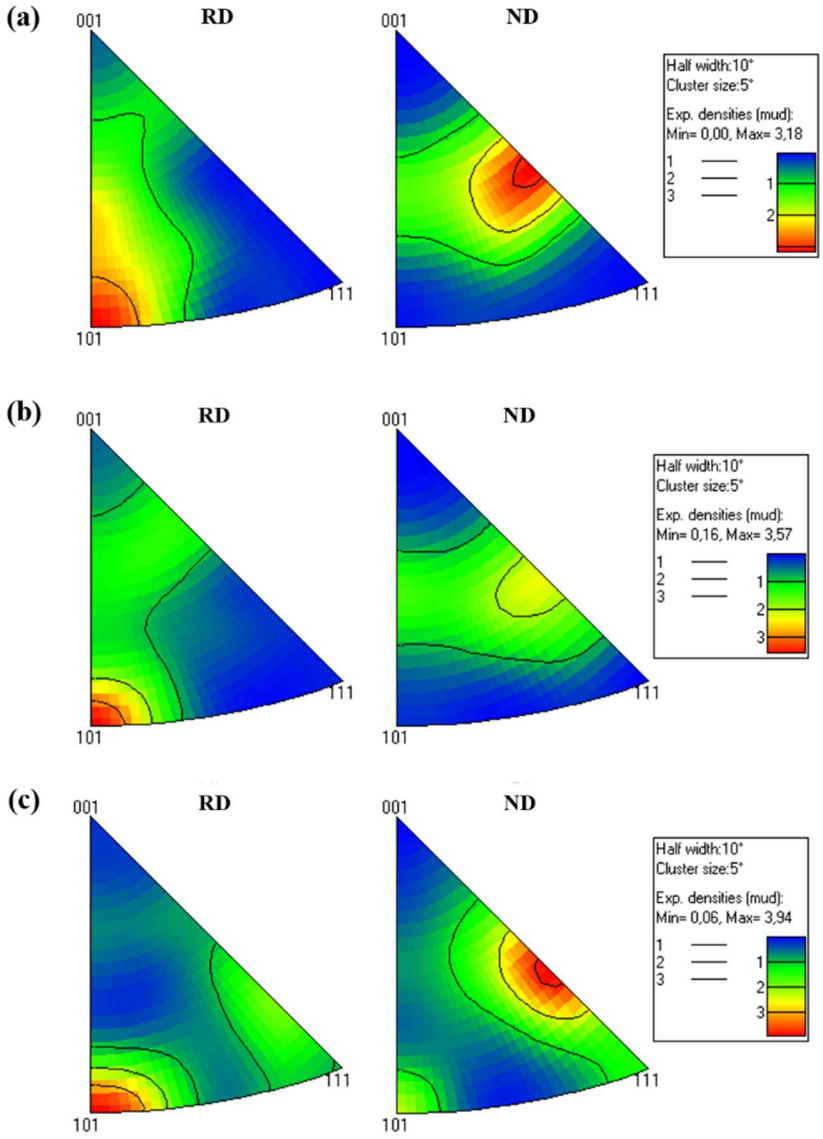

Fig. 4 EBSD inverse pole figures for recrystallized Ti2033 alloys at: (a) 973 K; (b) 1073 K; (c) 1173 K.

3.2 Grain size effect on superelasticity by nanoindentation

Combining EBSD orientation maps and nanoindentation tests, it is practically feasible to probe the superelasticity at the grain scale in localized region. The differently orientated grains show traceable grain boundaries under the microscope attached in nanoindentation platform, which facilitates the localization of the target grains with specific orientation identified from EBSD maps. Among the three specimens with different grain sizes, the areas with grains oriented or closely oriented in <113>$_\beta$ direction were selected and nanoindentation measurements were performed on those selected grains, so as to investigate the grain size effect on the superelastic behavior at grain scale.

To characterize the superelasticity of materials by nanoindentaion, the depth recovery ratio η_h and the work recovery ratio η_w can be extracted from nanoindentation load-depth

(*F-h*) curve [27], as highlighted in the schematic in Fig. 5a. Here, h_m denotes the maximum indentation depth, h_p denotes the permanently residual depth. The total energy W_t and the recoverable work W_{rc} are the integration area performed along the loading curve and the unloading curve, respectively. The magnitude of W_{rc} indicates the capability of a superelastic material to accommodate the deformation energy during indentation causing no damage [28].

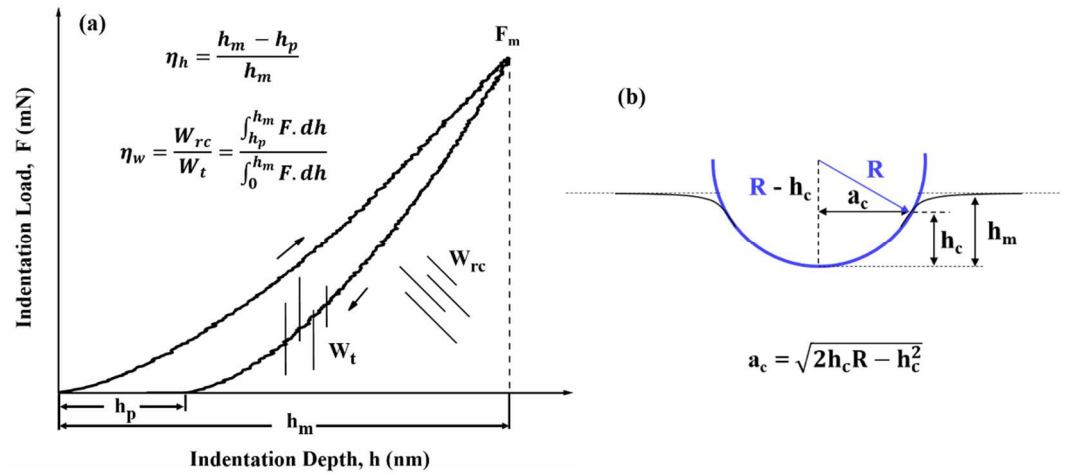

Fig. 5 (a) Schematic nanoindentation *F-h* curve and (b) schematic illustration of indentation upon loading showing the parameters used for the analysis.

Nanoindentation matrices were performed with maximum indentation depth h_m varying in the range of 50 - 1500 nm. The contact radius between the indenter and the specimen, $a_c=\sqrt{(2h_cR-h_c^2)}$, has been correspondingly calculated to be in range of 1.6 - 9.2 µm. Here, h_c is the contact depth and R is the tip radius, as shown in Fig. 5b. Therefore, it is worth noting that the real contact is mainly limited to the core of individual grains.

The η_h and η_w measurements were plotted as a function of h_m for the three Ti2033 specimens in Fig. 6. Each point represents the average value of at least 5 measurements. Magnitudes of η_h and η_w deviate initially from the 100% line at very shallow depths, instead of remaining at 100% value like the case of $\eta_{\varepsilon_{rec}}$ in Fig. 2b. It is probably due to the different loading conditions applied during tensile testing and during nanoindentation. The tensile testing corresponds to uniaxial stress condition while the nanoindentation produces rather complex loading conditions with triaxial stress state and constant change of the deformed volume. The stress of uniaxial tension testing is applied homogeneously in bulk and increases gradually with applied strain $\varepsilon_{applied}$, whereas during nanoindentation the spatial stress field under indenter tip is distributed radially, decreasing along the radial direction. Various studies [27, 29-31] modeled the deformation process underneath the indenter tip using four concentric shells: a fully transformed and plastically deformed martensite region

right beneath the tip, surrounded by a fully transformed and reversible martensite region, a partially transformed region and an untransformed parent β phase region. Therefore, once the stress state beneath the indenter tip is beyond the critical stress for dislocation slips σ_{CSS}, plastic deformation occurs and, therefore, the recoverability decreases, even at very shallow h_m.

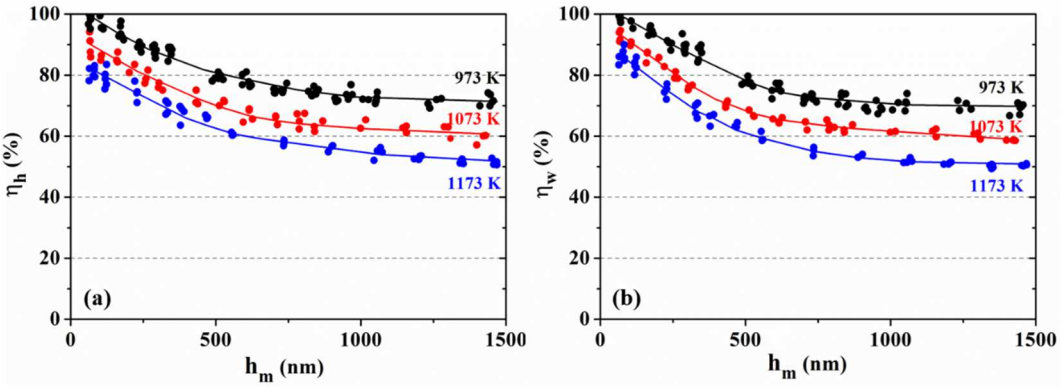

Fig. 6 Variations of depth recovery ratio η_h (a) and work recovery ratio η_w (b) versus maximum indentation depth h_m for Ti2033 specimens recrystallized at 973 K, 1073 K and 1173 K, respectively.

Besides, it is also shown that the recovery ratios, η_h and η_w, for the three Ti2033 alloys behave in the same way: decrease dramatically at low depths and saturate gradually at high depths. The values of η_h and η_w vary from 100% to 70% for the Ti2033-973K alloy, from 95% to 60% for the Ti2033-1073K alloy, and from 82% to 50% for the Ti2033-1173K alloy, respectively. By comparison, the Ti2033 alloy subjected to different heat treatments demonstrates the superelasticity characterized by nanoindentation in the following sequence: Ti2033-973K > Ti2033-1073K > Ti2033-1173K, which is in agreement with the macroscale recovery responses evaluated by tensile tests.

Nanoindentation is sensitive enough to probe the influence of grain size on the recoverability. The grain size indeed affects the superelasticity in Ti2033 alloys. The Ti2033-973K alloy with the smallest grain size exhibits the highest values of η_h and η_w, showing the highest superelasticity. Similar observation has been reported in β Ti-20Zr-12Nb-2Sn alloy [12]. It is due to that the critical stress for SIM transformation σ_{SIM} for the Ti2033-973K alloy has the lowest value and it increases with the increasing grain size tailored by heat treatments, as discussed above. It has been sufficiently evidenced that the σ_{SIM} depends on various factors, such as alloying elements [32], test temperature [20], presence of second phase [26, 33, 34], the strain rate [35], and grain size of β phase [16, 36-38]. In the present study, the focus is mainly on the analysis of the grain size effect on the σ_{SIM}. Several studies have made the supportive reports in agreement with our observations. Bhattacharjee et al. [16] pointed out that the σ_{SIM} increases with increasing β grain size up to

300 μm in Ti-10V-2Fe-3Al alloy. The dependence of σ_{SIM} on β grain size is related to the free energy changes for the SIM transformation. Similarly, Gil et al. [37] observed a linear increase in σ_{SIM} with increasing grain size. The elastic energy stored in grain boundary favors SIM transformation. The transformed martensite interacts with grain boundaries, increases the local elastic energy, and promotes the nucleation of new martensite. Wayman et al. [39] also stated that grain boundaries could act as one of the most preferential nucleation sites in martensitic transformation. Thus, grain refinement with higher density of grain boundaries facilitates the SIM transformation.

In addition, the grain size influences the relative mobility of dislocations in the parent and martensitic phases since the grain boundaries act as barriers for the dislocation movements. Grain refinement increases the critical stress for dislocation slips σ_{CSS}, and thus enhances the resistance to permanent plasticity deformation. Larger difference between the critical stresses for plasticity deformation and for SIM transformation results in a larger recovery strain in superelastic Ti-Nb-Ta alloy [40].

Therefore, it can be concluded that the higher critical stress for dislocation slips σ_{CSS} and the lower critical stress for SIM transformation σ_{SIM} contribute to the excellent superelasticity with a larger recovery strain in Ti2033-973K alloy with the smaller grain size.

The indentation hardness H_{IT} and modulus E_{IT} as a function of h_m have been extracted according to Oliver-Pharr method [41], and plotted for the three Ti2033 alloys in different grain sizes in Fig. 7. The smaller the grain size, the more grain boundaries underneath the indenter tip. For instance, in the case of Ti2033-973K, the highest density of grain boundaries will be involved during the indentation process. It is shown that Ti2033-973 K with smallest grain size exhibits the highest H_{IT} and the lowest E_{IT}.

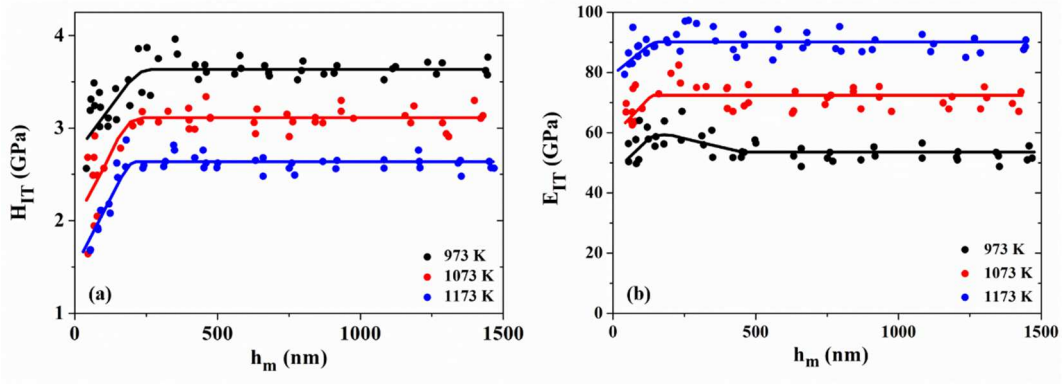

Fig. 7 Indentation hardness H_{IT} (a) and modulus E_{IT} (b) versus maximum indentation depth h_m for Ti2033 specimens recrystallized at 973 K, 1073 K and 1173 K, respectively.

The variation of indentation hardness versus grain size is in agreement with Hall-Petch relationship, which is also called grain refinement strengthening effect. This strengthening is attributed to the blockage of dislocation motions by the high density of grain boundaries. For

superelastic materials involving the SIM transformation, indentation hardness reflects not only the resistance for the plastic deformation, but also the resistance for the phase transformation, and indentation modulus is the apparent modulus associated with the transformed volume fractions of β and α″ phases. The Ti2033-973 K alloy shows lowest E_{IT}, probably due to its more prominent superelastic recovery accompanied by reversible SIM transformation that makes the material soft from the pseudo-elastic view.

4 Conclusion

In the present study, the superelastic Ti-20Zr-3Mo-3Sn (at. %) alloy was elaborated and subjected to different heat-treatments, and their microstructure presented the same strong $\{113\}_{\beta}<110>_{\beta}$ recrystallization texture but different average grain sizes were evidenced by EBSD. Investigation was performed to shed lights on the β grain size effect on the superelastic and mechanical properties. The main conclusions were made as follows:

(1) The evolution in the magnitude of the superelastic response probed by nanoindentation is in agreement with that measured by tensile tests. It confirms that nanoindentation can be used as an efficient tool to characterize the superelasticity and is sensitive enough to probe the grain size effect on the superelasticity.

(2) The superelastic behavior based on the reversible stress-induced martensitic transformation can be influenced by the grain size. The small-sized grains favor the martensitic transformation, resulting in high superelasticity.

(3) The alloy with smallest grain size exhibits the highest H_{IT} and the lowest E_{IT}.

Acknowledgements

Y. Zhou acknowledges the China Scholarship Council (CSC) for her Ph.D financial support (No. 201701810085). The authors also acknowledge the SCANMAT platform of the University of Rennes for providing access to SEM facilities.

References

[1] L. Héraud, P. Castany, D. Lailllé, T. Gloriant, In Situ Synchrotron X-ray Diffraction of the Martensitic Transformation in Superelastic Ti-27Nb and NiTi Alloys: A Comparative Study, Materials Today: Proceedings, 2 (2015) S917-S920.

[2] Y. Yang, P. Castany, M. Cornen, F. Prima, S.J. Li, Y.L. Hao, T. Gloriant, Characterization of the martensitic transformation in the superelastic Ti–24Nb–4Zr–8Sn alloy by in situ synchrotron X-ray diffraction and dynamic mechanical analysis, Acta Materialia, 88 (2015) 25-33.

[3] S. Miyazaki, H.Y. Kim, H. Hosoda, Development and characterization of Ni-free Ti-base shape memory and superelastic alloys, Materials Science and Engineering: A, 438 (2006) 18-24.

[4] Y. Al-Zain, H.Y. Kim, H. Hosoda, T.H. Nam, S. Miyazaki, Shape memory properties of Ti–Nb–Mo biomedical alloys, Acta Materialia, 58 (2010) 4212-4223.

[5] J. Fu, A. Yamamoto, H.Y. Kim, H. Hosoda, S. Miyazaki, Novel Ti-base superelastic alloys with large recovery strain and excellent biocompatibility, Acta Biomaterialia, 17 (2015) 56-67.

[6] M.F. Ijaz, H.Y. Kim, H. Hosoda, S. Miyazaki, Effect of Sn addition on stress hysteresis and superelastic properties of a Ti–15Nb–3Mo alloy, Scripta Materialia, 72 (2014) 29-32.

[7] J.J. Gao, I. Thibon, D. Laillé, P. Castany, T. Gloriant, Influence of texture and transformation strain on the superelastic performance of a new Ti–20Zr–3Mo–3Sn alloy, Materials Science and Engineering: A, 762 (2019) 138075.

[8] M.F. Ijaz, H.Y. Kim, H. Hosoda, S. Miyazaki, Superelastic properties of biomedical (Ti–Zr)–Mo–Sn alloys, Materials Science and Engineering: C, 48 (2015) 11-20.

[9] H. Kim, Y. Ikehara, J.I. Kim, H. Hosoda, S. Miyazaki, Martensitic transformation, shape memory effect and superelasticity of Ti–Nb binary alloys, Acta Materialia, 54 (2006) 2419-2429.

[10] H.Y. Kim, T. Sasaki, K. Okutsu, J.I. Kim, T. Inamura, H. Hosoda, S. Miyazaki, Texture and shape memory behavior of Ti–22Nb–6Ta alloy, Acta Materialia, 54 (2006) 423-433.

[11] T. Waitz, T. Antretter, F.D. Fischer, N.K. Simha, H.P. Karnthaler, Size effects on the

martensitic phase transformation of NiTi nanograins, Journal of the Mechanics and Physics of Solids, 55 (2007) 419-444.

[12] J.J. Gao, I. Thibon, P. Castany, T. Gloriant, Effect of grain size on the recovery strain in a new Ti‑20Zr–12Nb–2Sn superelastic alloy, Materials Science and Engineering: A, 793 (2020) 139878.

[13] F. Sun, S. Nowak, T. Gloriant, P. Laheurte, A. Eberhardt, F. Prima, Influence of a short thermal treatment on the superelastic properties of a titanium-based alloy, Scripta Materialia, 63 (2010) 1053-1056.

[14] Q. Sun, A. Aslan, M. Li, M. Chen, Effects of grain size on phase transition behavior of nanocrystalline shape memory alloys, Science China Technological Sciences, 57 (2014) 671-679.

[15] T. Grosdidier, Y. Combres, E. Gautier, M.J. Philippe, Effect of microstructure variations on the formation of deformation-induced martensite and associated tensile properties in a β metastable Ti alloy, Metallurgical and Materials Transactions A, 31 (2000) 1095-1106.

[16] A. Bhattacharjee, S. Bhargava, V.K. Varma, S.V. Kamat, A.K. Gogia, Effect of β grain size on stress induced martensitic transformation in β solution treated Ti–10V–2Fe–3Al alloy, Scripta Materialia, 53 (2005) 195-200.

[17] X. Bian, A.A. Gazder, A.A. Saleh, E.V. Pereloma, A comparative study of a NiTi alloy subjected to uniaxial monotonic and cyclic loading-unloading in tension using digital image correlation: The grain size effect, Journal of Alloys and Compounds, 777 (2019) 723-735.

[18] P.J.S. Buenconsejo, R. Zarnetta, A. Ludwig, The effects of grain size on the phase transformation properties of annealed (Ti/Ni/W) shape memory alloy multilayers, Scripta Materialia, 64 (2011) 1047-1050.

[19] Y. Zhou, A. Fillon, D. Laillé, T. Gloriant, Crystallographic anisotropy of the superelastic and mechanical properties of the Ti–20Zr–3Mo–3Sn alloy evidenced by nanoindentation at the grain scale, Journal of Alloys and Compounds, 892 (2022) 162112.

[20] T.W. Duerig, J. Albrecht, D. Richter, P. Fischer, Formation and reversion of stress induced martensite in Ti-10V-2Fe-3Al, Acta Metallurgica, 30 (1982) 2161-2172.

[21] T. Grosdidier, C. Roubaud, M.-J. Philippe, Y. Combres, The deformation mechanisms in the β-metastable β-Cez titanium alloy, Scripta Materialia, 36 (1997) 21-28.

[22] J.-L. Liu, H.-Y. Huang, J.-X. Xie, The roles of grain orientation and grain boundary characteristics in the enhanced superelasticity of Cu71.8Al17.8Mn10.4 shape memory alloys, Materials & Design, 64 (2014) 427-433.

[23] L.L. Pavón, E.L. Cuellar, S.V. Hernandez, I.E. Moreno-Cortez, H.Y. Kim, S. Miyazaki, Effect of heat treatment condition on microstructure and superelastic properties of Ti24Zr10Nb2Sn, Journal of Alloys and Compounds, 782 (2019) 893-898.

[24] H.Y. Kim, J.I. Kim, T. Inamura, H. Hosoda, S. Miyazaki, Effect of thermo-mechanical treatment on mechanical properties and shape memory behavior of Ti–(26–28)at.% Nb alloys, Materials Science and Engineering: A, 438-440 (2006) 839-843.

[25] H. Jabir, A. Fillon, P. Castany, T. Gloriant, Crystallographic orientation dependence of mechanical properties in the superelastic Ti-24Nb-4Zr-8Sn alloy, Physical Review Materials, 3 (2019) 063608.

[26] C. Li, X. Wu, J.H. Chen, S. van der Zwaag, Influence of α morphology and volume fraction on the stress-induced martensitic transformation in Ti–10V–2Fe–3Al, Materials Science and Engineering: A, 528 (2011) 5854-5860.

[27] Y. Zhou, A. Fillon, H. Jabir, D. Laillé, T. Gloriant, Investigation of the superelastic behavior of a Ti-16Zr-13Nb-2Sn sputtered film by nanoindentation, Surface and Coatings Technology, (2020) 126690.

[28] R. Liu, D.Y. Li, Y.S. Xie, R. Llewellyn, H.M. Hawthorne, Indentation behavior of pseudoelastic TiNi alloy, Scripta Materialia, 41 (1999) 691-696.

[29] C. Maletta, F. Furgiuele, E. Sgambitterra, M. Callisti, B. Mellor, R. Wood, Indentation response of a NiTi shape memory alloy: modeling and experiments, Frattura ed Integrità Strutturale, 6 (2012) 5-12.

[30] Q. Kan, W. Yan, G. Kang, Q. Sun, Oliver–Pharr indentation method in determining elastic moduli of shape memory alloys—A phase transformable material, Journal of the Mechanics and Physics of Solids, 61 (2013) 2015-2033.

[31] G.A. Shaw, D.S. Stone, A.D. Johnson, A.B. Ellis, W.C. Crone, Shape memory effect in nanoindentation of nickel–titanium thin films, Applied Physics Letters, 83 (2003) 257-259.

[32] A. Paradkar, S.V. Kamat, A.K. Gogia, B.P. Kashyap, Effect of Al and Nb on the trigger stress for stress-induced martensitic transformation during tensile loading in Ti–Al–Nb

alloys, Materials Science and Engineering: A, 487 (2008) 14-19.
[33] A. Paradkar, S. Kamat, A. Gogia, B. Kashyap, Effect of Volume Fraction of Primary α_2 on the Trigger Stress for Stress-Induced Martensitic Transformation in Two-Phase Ti-Al-Nb Alloys, Metallurgical and Materials Transactions A, 39 (2008) 2086-2094.
[34] Y. Yang, P. Castany, E. Bertrand, M. Cornen, J.X. Lin, T. Gloriant, Stress release-induced interfacial twin boundary ω phase formation in a β type Ti-based single crystal displaying stress-induced α" martensitic transformation, Acta Materialia, 149 (2018) 97-107.
[35] A. Paradkar, S.V. Kamat, The effect of strain rate on trigger stress for stress-induced martensitic transformation and yield strength in Ti–18Al–8Nb alloy, Journal of Alloys and Compounds, 496 (2010) 178-182.
[36] A. Paradkar, S. Kamat, A. Gogia, B. Kashyap, Trigger stress for stress-induced martensitic transformation during tensile deformation in Ti-Al-Nb alloys: Effect of grain size, Metallurgical and Materials Transactions A, 39 (2008) 551-558.
[37] F.J. Gil, J.A. Planell, Behaviour of normal grain growth kinetics in single phase titanium and titanium alloys, Materials Science and Engineering: A, 283 (2000) 17-24.
[38] M.-H. Cai, C.-Y. Lee, Y.-K. Lee, Effect of grain size on tensile properties of fine-grained metastable β titanium alloys fabricated by stress-induced martensite and its reverse transformations, Scripta Materialia, 66 (2012) 606-609.
[39] C. Wayman, H. Bhadeshia, Phase transformations, nondiffusive, in: Physical Metallurgy, Elsevier, 1996, pp. 1507-1554.
[40] H.Y. Kim, S. Hashimoto, J.I. Kim, T. Inamura, H. Hosoda, S. Miyazaki, Effect of Ta addition on shape memory behavior of Ti–22Nb alloy, Materials Science and Engineering: A, 417 (2006) 120-128.
[41] W.C. Oliver, G.M. Pharr, Measurement of hardness and elastic modulus by instrumented indentation: Advances in understanding and refinements to methodology, Journal of Materials Research, 19 (2004) 3-20.